



Investigating the Theory, Optics and Detector for WISP detection in ALPS

Yixuan Zhang

Imperial College London, UK

Supervisor: Dr. Axel Lindner

8 September 2015

Abstract

In the ALPS-II, I have contributed to all the fields of this project: theory, optics and detector. The theory of calculating the probability of a photon converting an axion or axion like particle using QED has been studied and reproduced and the sensitivity of the ALPS has been estimated. Research on cavity has been carried out by building the optics and aligning the system. The efficiency of coupling light into an optical fibre has been increased by 10% by using walking-the-beam method and a competitive game was designed and built using Arduino for the DESY open day. Finally, for detector studies, a few tests were performed to investigate the unexpected peak in quantum efficiency test 4 with wavelength of 1550nm. The black body photons were simulated using Python with two different methods for investigating the external inferred sources. Tests on the temperature gradient of the optical fibre, light-tightness shielding and the protection for the fibre were also performed.

Contents

1. Introduction.....	1
2. Theory.....	1
2.1 Hidden photons and minicharged particles.....	1
2.2 Light shining through a wall with $B=0$	4
3. Optics.....	6
3.1 Overview of the optics set up.....	6
3.2 Theory of Gaussian beam.....	7
3.3 Higher-order modes.....	7
3.4 Setting up the production cavity.....	8
3.5 Coupling light into an optical fibre.....	9
3.6 Coupling light into optical fibre game using Arduino.....	10
4. Detector.....	10
4.1 Transition Edge Sensor(TES) and current status.....	10
4.2 Simulation of the black body photon.....	12
4.3 Investigation of the black body photons sources.....	14
4.4 Temperature gradient of the optical fibre.....	15
4.5 Mechanical test for the protection of the optical fibre.....	15
5. Conclusion.....	16

1 Introduction

Many evidence from astronomy observations and theory calculations predict that about 25% of the known universe is made up of dark matter (DM) while only 4.9% of the universe is ordinary matter[3][4]. Since then, physicists have been searching for DM particles using varies methods: astronomical observation, direct detection by scattering or colliding particles at high energy. Up to now, no definite signal for DM has been observed and the search for DM particles has become one of the most popular area in particle physics.

There are many good candidates from the extensions of the Standard Model, the most popular one is called WIMP with masses ranging from 100GeV to few TeV [5][6]. These arise from Supersymmetry and can be detected by scattering with nucleus [7]. However, in the ALPS experiment, we are searching for DM particles with mass at sub-eV level. Such weakly interacting sub-eV particle has been named as WISP (weakly interacting slim particle). Besides this phenomenological reasoning, it has strong theoretical supports from the paper “Mixing the photon with low-mass particles” written by Georg Raffelt and Leo Stodolsky [12] and many other theorists [8-11]. It is believed that a particle called axion or an axion like particle (alp) could be produced by a photon and as the photon is traveling towards a wall in the presence of a magnetic field, the axion or alp could recombine to form a photon behind the wall [13-17]. This is the famous experiment called the “Light shining through a wall” which is the basic concept of ALPS [21][22].

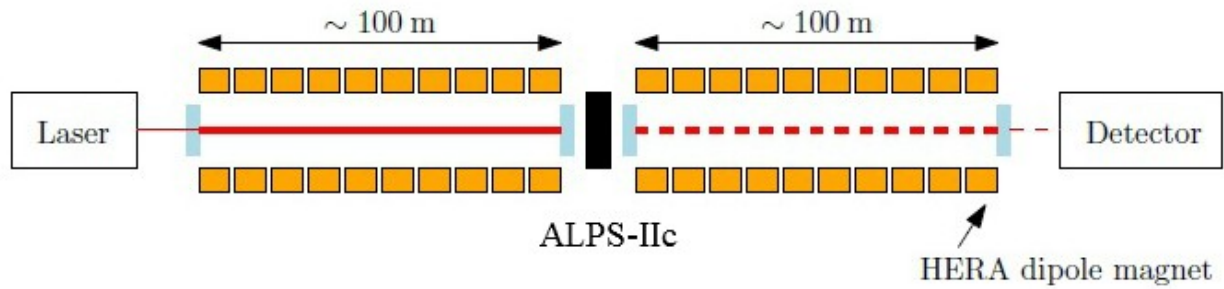


Figure 1: Layout of final stage of ALPS-II experiment at DESY.

The experimental search relies on the interaction between the WISP and the photon. Thus, optics is an ideal tool to search for WISPs, particularly in searching for tiny couplings to photons.

The ALPS group is divided into two main areas: Optics and Detector. The optics team is trying to fix the cavities and to increase the power build up so that the events could be enhanced inside the production cavity, and they are also building the optical setup for other parts. The detector team focuses on increasing the quantum efficiency of the TES (transition edge sensor) and attempting to explain the additional signal with unexpected wavelength. Also they are testing the effects that might influence the signals. The DAQ system is also under development.

In this report, I will go through the theory for the light shining through a wall experiment and also the estimation of the sensitivity for ALPS. Then I will present the setup for the production cavity and improvement on coupling the laser into optical fibre. Additionally, a competition game for DESY open day was also designed and made using Arduino. Finally, thermal tests for the detector and optical fibres will be shown. Simulations for the black body photons with different methods will be studied to further understand the unexpected signals.

2 Theory

2.1 Hidden photons and minicharged particles

A “hidden sector” of particles is predicted by many theories from the extension of Standard Model which transform trivially under the SM gauge group. In other words, they interact very weakly with

the “visible sector” of particles i.e. the SM particles. The main example is the axion which arises as Nambu-Goldstone bosons associated with breakdown of global symmetries. Further WISPs candidates such as hidden photons and minicharged particles, likewise, arise naturally in the models with extra Abelian U(1) gauge [19][20].

If the hidden sector particle has a two-photon vertex, it may be created by a photon under the presence of magnetic field [12]. Furthermore, this particle may be massless or have little mass, leading to a near-degeneracy with the photon. Therefore, a mixing between the particle and the photon is expected, similar to the neutrino mixing. Under the case of near-degeneracy, one needs to take care of the small effects which could be problematic even in vacuum. The QED effects will play an important role particularly in strong magnetic field [23-25]. As a result, one needs to take into account of this effects by using the Euler-Heisenberg effective Lagrangian [26], from which we could find the equation of motion of the hidden sector particle and thus its probability of being detected.

The theory proof was mainly based on [13] and under the guidance from Andreas Ringwald. Starting with the simplest model with two U(1) gauge groups, one being the electromagnetic group $U(1)_{\text{QED}}$, the other being the hidden sector group $U(1)_{\text{Hidden}}$ under which the SM particles all have zero charges. Apart from photons (A_μ), new Abelian gauge boson (B_μ) is introduced to represent this hidden particle and the Lagrangian allowed by symmetry would be [13]

$$L = -\frac{1}{4}F^{\mu\nu}F_{\mu\nu} - \frac{1}{4}B^{\mu\nu}B_{\mu\nu} - \frac{1}{2}\chi F^{\mu\nu}B_{\mu\nu} \quad (2.1)$$

where $F_{\mu\nu}$ is the field strength tensor for the visible sector $U(1)_{\text{QED}}$ gauge field A_μ (photons), ($B^{\mu\nu}$) is the field strength tensor for the hidden sector $U(1)_{\text{Hidden}}$ gauge field B_μ (the hidden photons), χ is an arbitrary parameter at low energy scale. The first two terms describe the kinetic terms for the photons and the hidden photons fields. As the field strength is gauge invariant for the U(1) gauge fields, the third term is allowed by the Lorentz and gauge symmetries which describes the interaction between the photons and the hidden photons. It's a non-diagonal kinetic term, so called the kinetic-mixing term.

We could diagonalise the kinetic terms by a shift

$$B^\mu \rightarrow \tilde{B}^\mu + \chi A^\mu \quad (2.2)$$

then the Lagrangian becomes

$$L = -\frac{1}{4}(1-\chi^2)F^{\mu\nu}F_{\mu\nu} - \frac{1}{4}\tilde{B}^{\mu\nu}\tilde{B}_{\mu\nu} \quad (2.3)$$

The Lagrangian is unaffected by this shift besides the normalisation of the gauge coupling is changed by a factor of $(1-\chi^2)$.

Similarly, if we assume that the hidden sector fermion h has a charge one under B^μ and we apply the shift (2.2) to the coupling term, we found that

$$e_h \bar{h} B h \rightarrow e_h \bar{h} \tilde{B} h - \chi e_h \bar{h} A h \quad (2.4)$$

where e_h is the hidden-sector gauge coupling. Thus, the hidden-sector now has a charge of

$$\varepsilon e = \chi e_h \quad (2.5)$$

where e is the gauge coupling of the electromagnetic field A_μ , ε is a fractional electric charge but not necessary to be an integer. For $\chi \ll 1$ (could be obtained in supersymmetry or string theory) [27], it is observed that $|\varepsilon| \ll 1$, and h becomes a minicharged particle.

All the above calculations were following the unbroken $U(1)_h$ symmetry for hidden photon. A mass term was added to break the symmetry

$$L_\mu = \frac{1}{2}\mu^2 B^\mu B_\mu \quad (2.6)$$

where μ is the mass of the hidden photons via Higgs mechanism. After the shift (2.2), the expression

$$L_\mu = \frac{1}{2} \mu^2 (\tilde{B}^\mu \tilde{B}_\mu - 2\chi \tilde{B}^\mu A_\mu + \chi^2 A^\mu A_\mu) \quad (2.7)$$

the photons and the hidden photons are mixed together to form a mixed mass term.

By introducing the propagator in the (A^μ, \tilde{B}^μ) basis, one can show that the minicharge is eliminated by the mass term when it is on shell. This is not the case when for off shell or massive photons (e.g. plasma).

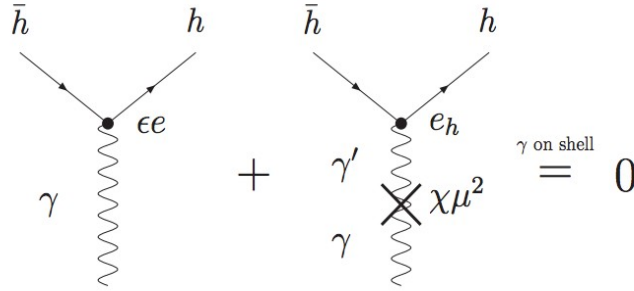


Figure 2: Feynman diagrams of coupling the photon into hidden-sector fermion h at which hidden photon is massive. The second diagram (due to the additional mass term (2.7)) cancels the first one (due to the shift (2.2)) if the external photon is massless and on shell.

The generalise form for the interaction between the photons and the hidden photons can be obtained by combining (2.1) and (2.6). We will look at a slightly more involved model, the MR model [1], which involves two hidden photons B_1^μ and B_2^μ . For simplicity, the following derivations will use matrix notations (A , B_1 , B_2) instead of the Lorentz indices.

$$L = -\frac{1}{4} F^T K F + \frac{1}{2} A^T M A \quad (2.8)$$

with

$$\text{kinetic mixing: } K = \begin{pmatrix} 1 & \chi & \chi \\ \chi & 0 & 0 \\ \chi & 0 & 0 \end{pmatrix}, \text{ mass mixing: } M = \begin{pmatrix} 0 & 0 & 0 \\ 0 & \mu^2 & 0 \\ 0 & 0 & 0 \end{pmatrix} \quad (2.9)$$

Applying the shift (2.2) to this new Lagrangian, the kinetic term can be diagonalised and leaves the electromagnetic gauge field unaffected. By analogy to (2.4) and applying (2.2) to both B_1 and B_2 , it can be shown that

$$e_h \bar{h} (B_1^\mu - B_2^\mu) \gamma_\mu h \rightarrow e_h \bar{h} [(\tilde{B}_1^\mu - \chi A^\mu) - (\tilde{B}_2^\mu - \chi A^\mu)] \gamma_\mu h = e_h \bar{h} (\tilde{B}_1^\mu - \tilde{B}_2^\mu) \gamma_\mu h. \quad (2.10)$$

It seems as if there is no interaction between the hidden photons and the ordinary photons. However, we should note that one of the hidden photons is massive. In the new basis $(A, \tilde{B}_1, \tilde{B}_2)$, the mass mixing term becomes

$$\tilde{M} = \begin{pmatrix} \chi^2 \mu^2 & -\chi \mu^2 & 0 \\ -\chi \mu^2 & \mu^2 & 0 \\ 0 & 0 & 0 \end{pmatrix} \quad (2.11)$$

In the first case with only one hidden photon, the mass term cancels the effects on the minicharges induced by massive photons. In the second case with two photons where one of them is massless, the effects on minicharges are unaffected and thus have an effective charge.

At high virtuality, the minicharge is not undone by the mass term and the two hidden photons behave as if they are massless. As a result, we could neglect the mass term.

2.2 Light shining through a wall with B=0

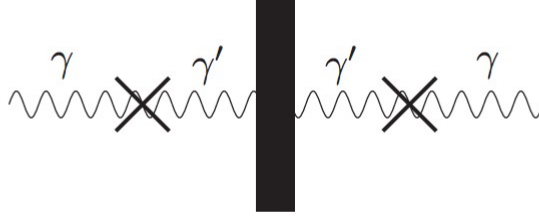


Figure 3: Light shining through a wall experiment with photon converting into hidden photons and is reconverted back behind the wall.

We have discussed in the previous section of how the non-diagonal mass matrix contributes to the effective charge of the hidden-section fermion by considering a photon changes into a hidden photon. As shown in figure 3, the photon may convert into a hidden photon as it propagating towards a wall. Since the hidden photon \tilde{B} does not interact with ordinary matters, it directly passes through the wall and then reconverted into a photon afterwards.

This process is similar to neutrino oscillation in which the particle oscillating between photon and hidden photon. Likewise, the interaction eigenstate is different from the propagation eigenstate.

By writing down the equation of motion, we are able to obtain the probability of a photon propagating via this process. In the shifted basis, we assume the photon is propagating in z direction

$$[(\omega + \partial_z^2)I - \mu^2 \tilde{M}] \begin{pmatrix} A \\ \tilde{B} \end{pmatrix} = \left[(\omega + \partial_z^2) \begin{pmatrix} 1 & 0 \\ 0 & 1 \end{pmatrix} - \mu^2 \begin{pmatrix} \chi^2 & -\chi \\ -\chi & 1 \end{pmatrix} \right] \begin{pmatrix} A \\ \tilde{B} \end{pmatrix} = 0 \quad (2.12)$$

where ω is the frequency of the propagating photon and ∂_z^2 is the second derivative in the z direction. Recall that A represents the field of photon and \tilde{B} represents the field of the massive hidden photon. This is the case with only one massive hidden photon which is completely equivalent to the case with two hidden photons in the MR model [1], since the mass matrix is only non-vanishing with the photon and the first hidden photon and thus the second hidden photon does not mix with the photon (when B=0).

Subbing the trial solution $\begin{pmatrix} a \\ b \end{pmatrix} e^{-i(\omega t - kz)}$ into (2.12), the two eigenstates are found to be

$$v_1 = \begin{pmatrix} 1 \\ \chi \end{pmatrix} \exp(-i(\omega t \pm k_1 z)) \quad , \quad \text{with} \quad k_1^2 = \omega^2 \quad (2.13)$$

$$v_2 = \begin{pmatrix} -\chi \\ 1 \end{pmatrix} \exp(-i(\omega t \pm k_2 z)) \quad , \quad \text{with} \quad k_2^2 = \omega^2 - \mu^2 - \chi^2 \quad (2.14)$$

where k is the wavenumber and z is the distance of propagation. The higher order in (2.14) is neglected as it is very small.

Initially, $z = 0$, $t = 0$ and it is in a pure photon state [13], i.e. $\chi = 0$. Thus, the superposition of the wave could be obtained as

$$V(0, 0) = A_0 \begin{pmatrix} 1 \\ 0 \end{pmatrix} = A_0 \left(\frac{1}{1 + \chi^2} v_1(0, 0) - \frac{\chi}{1 + \chi^2} v_2(0, 0) \right) \quad (2.15)$$

And the probability of a photon remaining unchanged is

$$P_{\gamma \rightarrow \gamma} = \frac{|V_1(z, t)|^2}{|A_0|^2} = 1 - 4\chi^2 \sin^2\left(\frac{\Delta k z}{2}\right) + O(\chi^4) \quad (2.16)$$

where

$$\Delta k = k_1 - k_2 \approx \frac{\mu^2}{2\omega} \quad \text{for } \mu \ll \omega. \quad (2.17)$$

Therefore, the probability of the photon converting into a hidden photon will be

$$P_{\gamma \rightarrow \gamma'}(z) = 1 - P_{\gamma' \rightarrow \gamma}(z) = 4\chi^2 \sin^2\left(\frac{\mu^2}{2\omega} z\right) = P_{\gamma' \rightarrow \gamma}(z) \quad (2.18)$$

For a single photon event, there will be only one photon passing through and one photon reconverted on the back of the wall. Thus, the probability of one photon detection will be

$$P_{trans} = P_{\gamma \rightarrow \gamma'} P_{\gamma' \rightarrow \gamma} = 16\chi^4 \sin^2\left(\frac{\mu^2 l_1}{2}\right) \sin^2\left(\frac{\mu^2 l_2}{2}\right) \quad (2.19)$$

with l_1, l_2 being the lengths before the wall and after the wall.

If a pair of mirrors which forms a cavity is placed in front of the wall, the probability of detecting the photon behind the wall is enhanced.

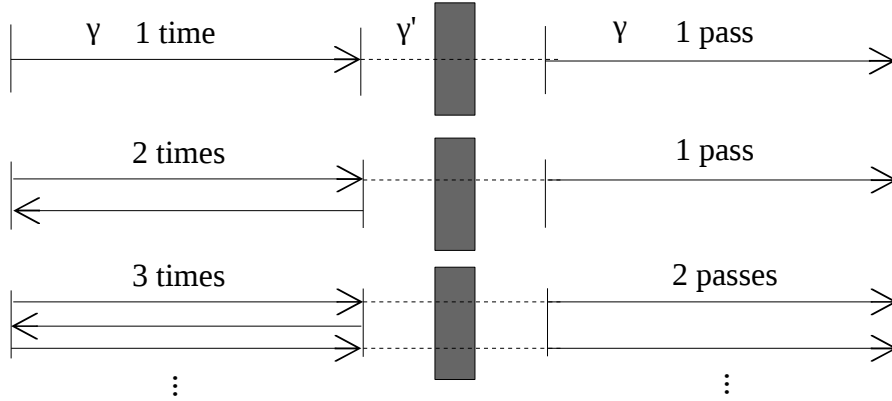


Figure 4: The photons are reflecting within the cavity, only the ones that are propagating towards the wall will have a chance of passing through the wall.

If the photon beam is reflected by the mirrors for N_{pass} times, the number of photons crossing the wall will be $(N_{pass} + 1)/2$ and the probability will be enhanced by this factor. Thus, the number of photons being detected will be

$$N = N_0 \eta \frac{N_{pass} + 1}{2} P_{trans} \quad (2.20)$$

with N_0 number of initial photons and a detection efficiency of η (<1). This is the basic theory behind the ALPS experiment [28] without magnetic field where it has lengths of 4.21m both before and after the wall, the laser has power of 200W with 532nm wavelength. Since there's no cavities, the number of passes is just one. From these values, we can compute to find the limit for the ALPS.

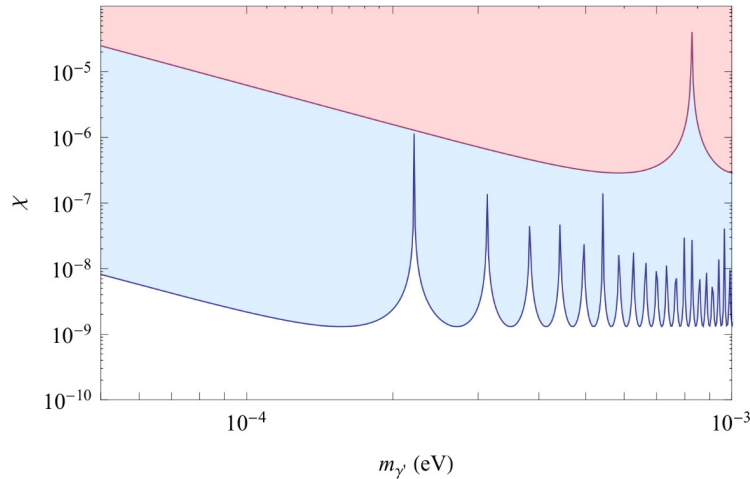


Figure 5: Hidden photon searches with LSW experiment for ALPS. The red region is the best sensitivity for ALPS-I and the blue region is for ALPS-II.

3 Optics

3.1 Overview of the optics set up

The heart of the whole experiment is the optics. With this powerful tool, we can explore more into the precision measurement in order to find the WISP particle. In the ALPS-II [2], it consists of three parts: the production, the central and the regeneration parts, corresponds to the table 1,2 and 3 respectively from the figure below.

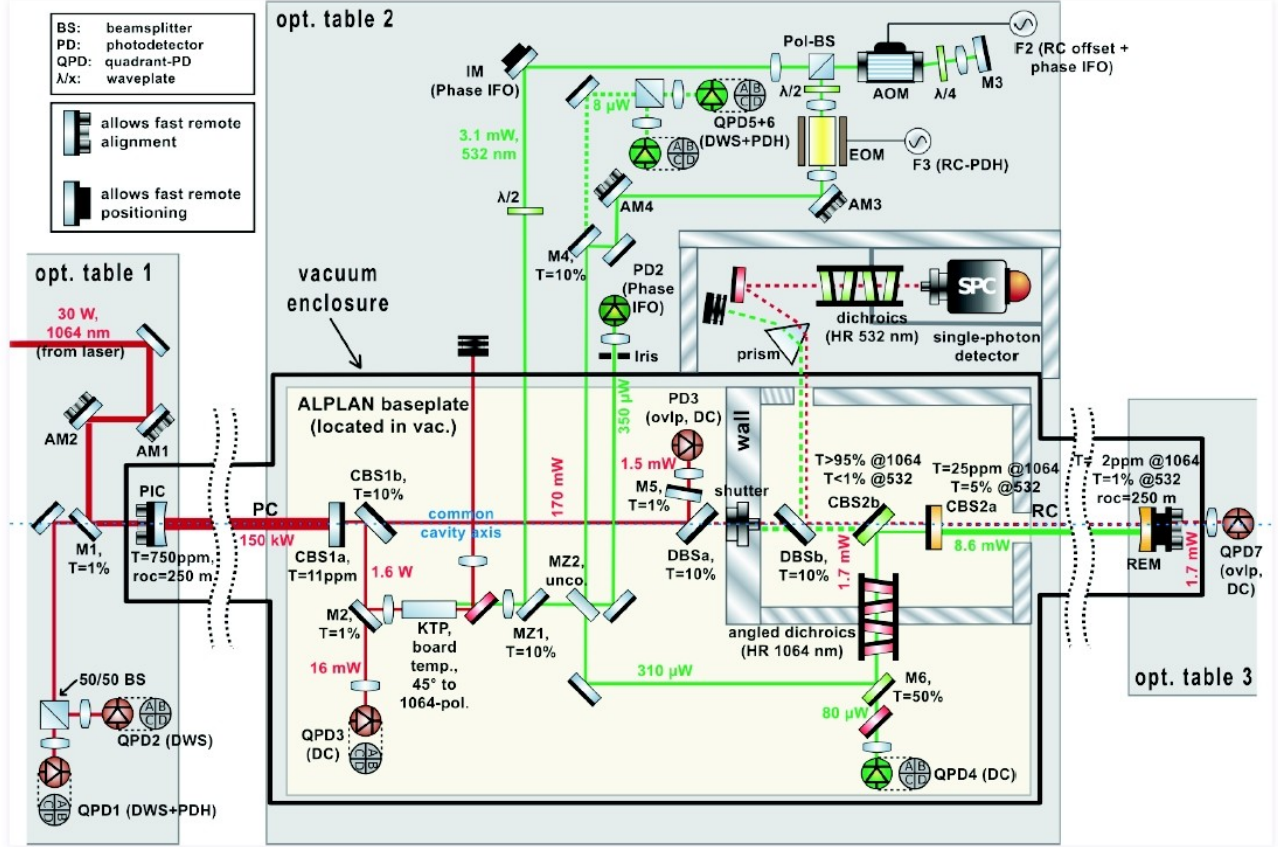


Figure 5: Optical layout of the ALPS-II.[2]

The initial laser beam has a power of 30W and a wavelength of 1064nm sitting on the table 1 which is then enhanced by the production cavity in between table 1 and 2. In the central part where the wall is situated, a reference beam with 532nm (half of the original beam) is produced from the initial laser beam and fed into the regeneration cavity in between table 2 and 3. This is used to tune the two cavities to be the same cavity length and also vibration frequency [36]. The potential axion particle signal will be enhanced at the regeneration cavity and will be directed towards the detector on the table 2. The 532nm reference beam will go through the same path but will later be refracted by the prism. At the end, the axion photon will be focused into an optical fibre which is linked into the cryostat and will be directed to the Transition Edge Sensor(TES).

For this project, the task will be focusing on the optimisation of the production cavity and the the link between the optics and the detector by coupling the photons into the optical fibre. In order to do so, we need to first look at the theories behind the optics.

3.2 Theory of Gaussian beam

In the past studies, we normally expect a beam to be focused to an infinitesimal point by a focal lens. However, in reality, the beam does no focus to a single point, instead, it has a minimum width

which depends on its wavelength, beam size and the focal length [29][30].

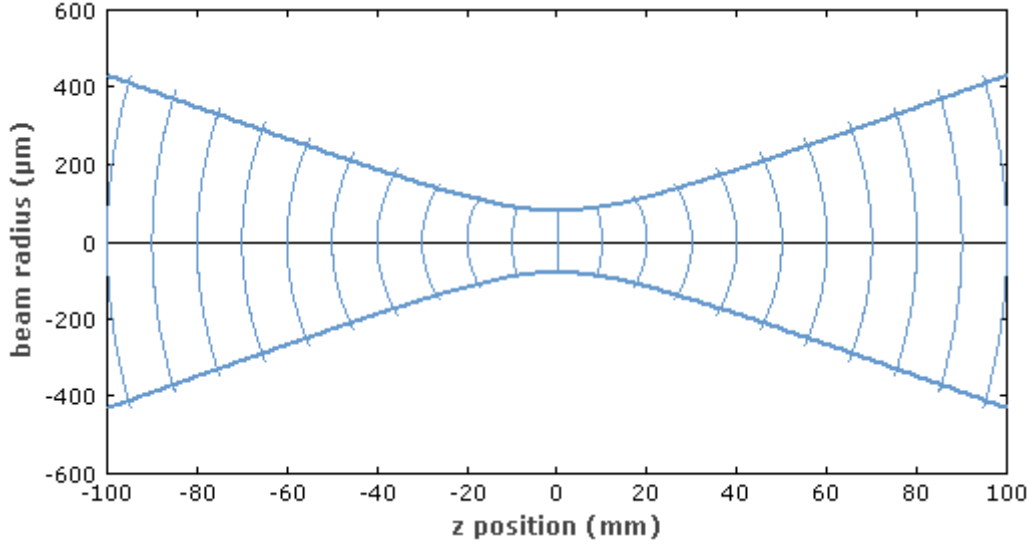


Figure 6: Gaussian beam with curved wavefront.

The Gaussian beams are normally considered to have relatively small divergence. In this case, the paraxial approximation can be applied so that as the beam is propagating through free space, it remains as a Gaussian, only the parameters of the beam will change along the path. One major parameter is the beam radius $w(z)$ which varies according to the distance. The beam size will converge to a certain width as it propagates and will diverge again, the point where it reaches the minimum is called the waist point and is governed by the formula

$$w(z) = w_0 \sqrt{1 + \left(\frac{z}{z_R}\right)^2} \quad (3.1)$$

with the Rayleigh length

$$z_R = \frac{\pi w_0^2}{\lambda} \quad (3.2)$$

where w_0 is the waist size of the beam. Within the Rayleigh length, the beam does not diverge significantly and a beam with large Rayleigh length is called the collimated beam. And the angle of divergence in the far field ($z \gg z_R$) will be

$$\theta = \frac{\lambda}{\pi w_0} \quad (3.3)$$

which indicates that the smaller the waist size, the more divergent the beam will be. Thus, in order to couple the beam into an optical fibre which has a very small diameter, we would need to optimise the parameters by using the relations above. To achieve this, we would need to use the optical components.

3.3 Higher-order modes

So far, we have only discussed about the Gaussian shape of beam. This is actually the fundamental mode among the possible solutions to the paraxial wave equation. The reason is that an imperfect laser beam is a superposition of the basis set of orthogonal solutions, it consists not only the Gaussian mode but also other higher order modes. If the laser beam shines through a cavity, according to the length of the cavity, the output beam will have different modes. This is due to that only certain modes will be resonant with the cavity. The most common modes in the laser system are the Hermite-Gauss modes [31], since there is a Cartesian reflection symmetry perpendicular to the propagation direction of the beam.

3.4 Setting up the production cavity

At the current stage, the team is researching on why they lose some of the laser intensity in the 10m long cavity. One of the possibilities is that the end mirror was flat during the testing. If the beam was not perfectly aligned, the beam would eventually leave the cavity which would result in intensity loss. Thus, we set up a production cavity with 10cm and to align the beam into the cavity with the Gaussian mode in order to diagnose the causes of this.

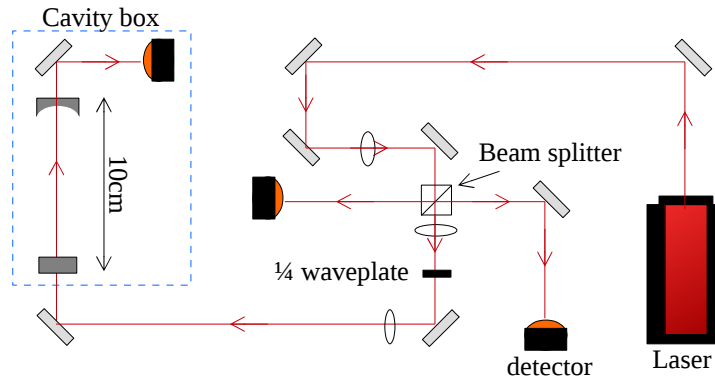


Figure 7: Optical setup for cavity.

The mirrors in the cavity box were partially transparent of which the closest one is flat and the end one is curved. The curved mirror was used to trap the laser beam inside the cavity and was partially transparent in order to align the system.

The purpose is to align the beam so that it is well collimated and the waist point is at the same place as the first cavity mirror in order to have a flat wavefront. The beam was simulated by a java script and it was found that the goal can be achieved by using three focal lenses at specific positions. By slightly adjusting the position of the last lens, the resultant beam will change the waist size and the position of its waist point. So a wincam was used to measure the sizes of the beam along the path for different positions and the data was collected for analysis. The waist size and position of the waist point were then calculated by using equations in section 3.2 to determine the suitable position of the last lens. After the optimisation of the lens position, the laser beam is then adjusted into the cavity. To avoid any back reflection from the cavity that could damage the laser source, a $\frac{1}{4}$ waveplate was used.

As mentioned in the previous section, the length of the cavity will determine whether the beam is Gaussian or higher-order mode. Another factor that can influence the mode is the incident angle of the laser with the first mirror. If the angle is tilted, even if the beam is a perfect Gaussian mode with no superposition of other modes, the cavity will see the beam as if it is higher-order mode. Therefore, the first step is to align the beam so that the back reflection from the mirrors is on the same path as the incoming beam and the shape of the beam will be shown by the camera at the end if it is properly aligned.



Figure 8: Gaussian mode beam shown on the camera.

It was observed to be Gaussian mode and was flashing on the screen with different sizes. The beam was still diverging inside the cavity and the end mirror transmits a small percentage of light. As a result, the output beam would be of different sizes according to how many turns the beam was reflected inside the cavity.

An offset was attached to the cavity mirrors to fix the length of the cavity in order to keep the Gaussian mode. Next step, further understanding on the cavity will be investigated.

3.5 Coupling light into an optical fibre

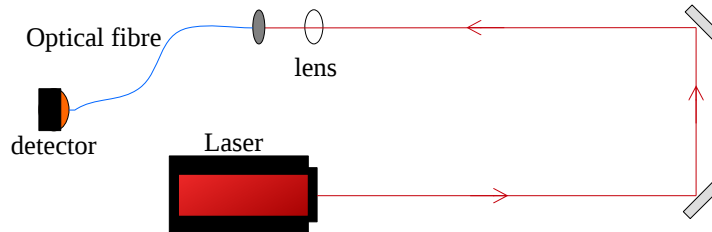


Figure 9: Optic set up for coupling light into optical fibre.

This is the connection between the axion generation part and the signal detection part. It is desirable to achieve high coupling efficiency ideally above 90% [37] and so far it was achieved to be 53%. The task is to increase the efficiency while keeping the beam as Gaussian mode.

A He-Ne laser was used which has a wavelength of 534nm and a waist size of $362\mu\text{m}$ at 2cm after the aperture. Two mirrors were used to introduced 4 more degrees of freedom in order to align the beam. A lens with focal length 25.4mm was used to focus the beam into the optical fibre which had an aperture of $8.2\mu\text{m}$ and then is connected to a powermeter to read the output. Similar to the section above, the positions of the lens and the aperture of the optical fibre were simulated to maximise the coupling efficiency. In order to have a Gaussian mode, the waist size of the beam needs to be the same as the aperture of the optical fibre. By comparing with the intensity of the input laser, we will be able to calculate the efficiency. To ignore the absorption by the poor quality of the mirrors, the input intensity was measured to be $0.905 \pm 0.005\text{mW}$ just before the lens.

To align the beam, a 1064nm laser beam was fed in from the end of the fibre and adjusted to match with the incoming beam by the two mirrors. The lens was also adjusted so that the 1064nm laser beam is well collimated. Then the reference laser was removed, and the fibre is connected to the powermeter. By varying the angles of the mirrors, the output could reach a maximum value. Finally, a technique called walking the beam was used to further optimise the efficiency.

The maximum attempt value was $0.560 \pm 0.005\text{mW}$. Thus, the percentage of efficiency was obtained to be $61.9 \pm 0.6\%$. The uncertainty mainly came from the precision of the powermeter.

There were other factors need to be noticed that might contribute to the loss in efficiency. First observation was that there were some reflection from the aperture of the optical fibre which indicated that not all the beam was focused into the fibre. Due to the limitation of the lens, only one lens with 25.4mm was used. To optimise the result, more lens could be used to create a suitable waist size. Second observation was that the fibre was glowing in the dark, the more the fibre was bent, the brighter the glowing would be. This could be explained by the geometry of the light passing through the optical fibre. As soon as the incident angle to the side of the core is larger than the critical angle, the light will be refracted out from the core of the fibre which will result in loss in efficiency. One solution could be to keep the optical fibre as straight as possible, avoiding large curvature.

The significance of this observation was that in this experiment the laser beam was visible light and the problem could be directly notified. However, in the ALPS-II, the laser is in the inferred region

and it won't be obvious to see such effect.

3.6 Coupling light into optical fibre game using Arduino

This project was designed for the DESY open day. With the same principle as described above, a competitive game was designed and built.

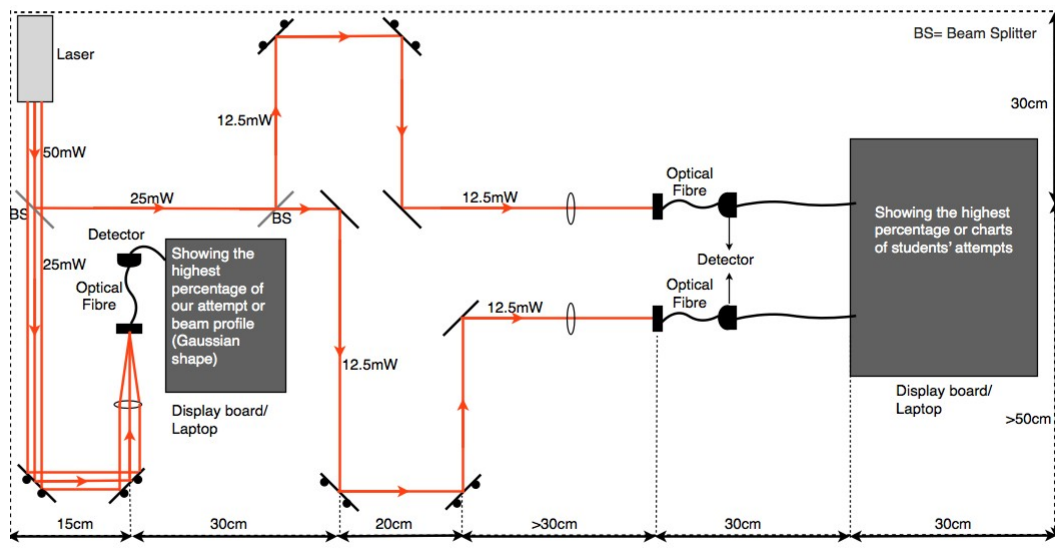


Figure 10: Competitive game for DESY open day.

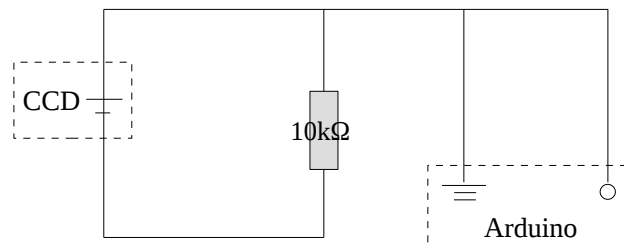


Figure 11: Electric circuit that translate the signals from the detector to computer.

A class 2 laser was used as the light source and two pairs of adjustable mirrors were placed on each side of the optical table. Each path followed the same method as the previous section. Instead of connecting to a powermeter, the CCD detector was connected to a circuit board. The signal from the detector was then transferred into the computer via the Arduino.

A GUI for displaying the results were created and an animation for the particle flow was simulated according to the amount of photons passing through. By adjusting the pairs of mirrors, visitors can compete with each other in a limited amount of time.

4 Detector

4.1 Transition Edge Sensor(TES) and current status

The transition edge sensor (TSE) is a type of cryogenic particle detector [32]. It operates at very low temperature by using the principle of superconducting phase transition where a small raise in the temperature would result in a dramatic increase in its resistance.

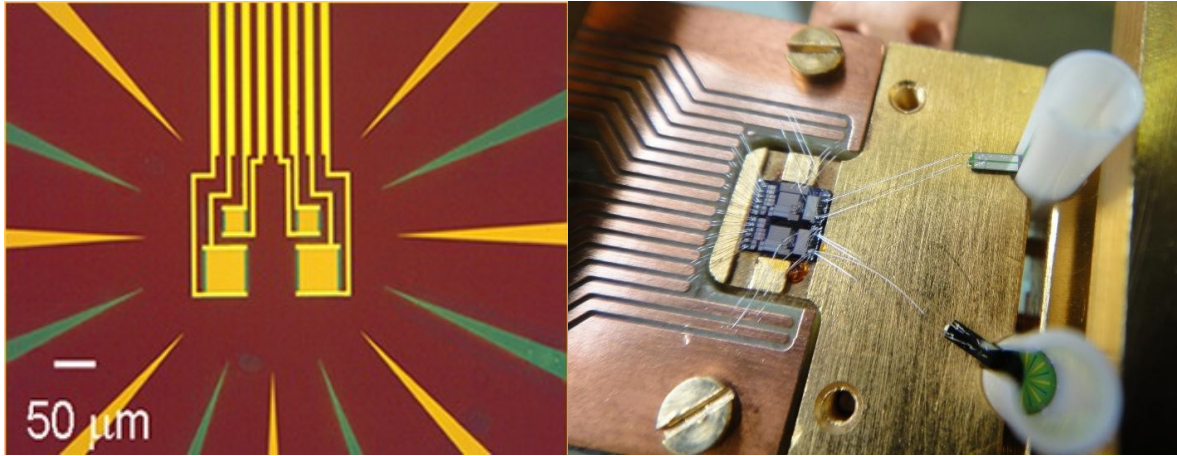


Figure 12: TES (left)[3], two TESes with the readout system SQUID.

The TES for ALPS-II was specially made by NIST and was designed to measure the inferred single-photon in the environment of 80mK [33][34]. It is connected with the optical fibre and the photons can be directly detected by the TES shown in the figure 12.

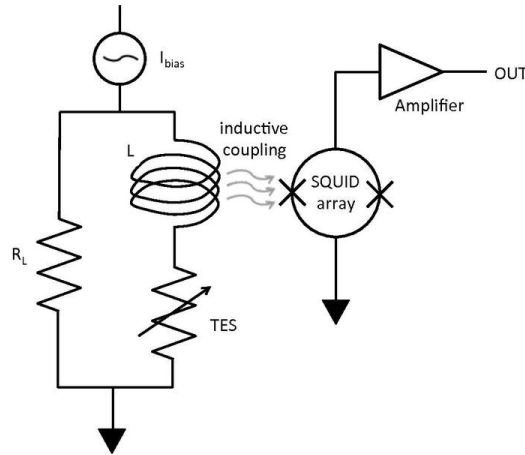


Figure 13: Readout system of TES, the TES-SQUID circuit.

A voltage is applied to put the TES into its self-biased region where the dissipated power in the device is constant. When a photon enters the TES, the resistance of the TES increases and the current in the circuit drops. Thus, the Joule power will decrease and the system will be cooled back to equilibrium in the self-biased region. In the readout system, the TES is in series with the coil L which is inductively coupled to the SQUID array [35]. As soon as there is a change in the TES current, the SQUID will see an input flux whose output will be further amplified and to be read out under room temperature condition.

The temperature of the TES is cooled by the Adiabatic Demagnetization Refrigerator (ADR) down to 80mK inside a cryostat where the cooling system and pressure sensor are built in to monitor the environment for the detector. It is obviously much more difficult to set up and operate than CCD, but it can promise a very high quantum efficiency $\sim 98\%$, high time/energy resolution and has a very small intrinsic background [33]. These properties make TES ideal for detecting low counts of photons for ALPS-II.

The current research on the detector is to test the performance of the TES and to diagnose the origin of the low efficiency. Also an unknown peak of 1550nm wavelength was observed in the previous run, it was tested via simulation and experimental approach to explain this phenomenon in order to eliminate this effect.

4.2 Simulation of the black body photon

Since the laser that we are using is with 1064nm, the 1550nm peak was unexpected from the signal. It is very likely produced by the black body photons [38] emitted by a heating body which could enter the optical fibre either from the entrance by outer sources or from inside by fibre itself. If the black body photons are coming from the entrance, it may be due to the input laser or the reflection from the environment. If the black body photons are formed by the fibre itself, it may be due to the temperature of the environment or by other heating sources that could heat up the fibre. To see how the black body photon counts vary with the temperature, a simulation was done by Python to for investigation. Two methods of approach were performed to compare and conclude the result.

First method is to start with the black body distribution of photon energies

$$u(\omega) d\omega = \frac{\hbar}{\pi^2 c^3} \frac{\omega^3 d\omega}{e^{\hbar\omega/kT} - 1} \quad (4.1)$$

and we get the occupation number with the approximation of $\hbar\omega/kT \gg 1$ (in our case $\hbar\omega/kT \approx 50$) and is simplified to

$$n(\omega) d\omega \approx \frac{\omega^2}{\pi^2 c^3} e^{-\hbar\omega/kT} d\omega \quad (4.2)$$

By integrating this from ω_1 to ω_2 , and by replacing ω to $x = \hbar\omega/kT$, we obtain an expression for the number of black body photons

$$N = \frac{k^3 T^3}{\hbar^3 \pi c^3} (x_1^2 - x_2^2 + 2(x_1 - x_2) + 2)(e^{-x_2} - e^{-x_1}) \quad (4.3)$$

with λ_1 to be the lower value of the wavelength, $\lambda_1 = \langle \lambda \rangle - \Delta\lambda$ where $\Delta\lambda = \langle \lambda \rangle \times 8\%$ is the energy resolution and $x_1 = \frac{1}{\lambda_1} \frac{\hbar c}{kT}$.

For the second method, we use Gauss-Legendre method [39] for evaluating the integral for the spectral radiance [38]

$$L = \int_{\lambda_1}^{\lambda_2} \frac{2hc^2}{\lambda^5} \frac{1}{\exp(\frac{hc}{k\lambda T}) - 1} d\lambda \quad (4.4)$$

with unit of $W \cdot m^{-2} \cdot sr^{-1}$. And the number of black body photons entering the fibre s^{-1} can be calculated as

$$N_{bb} = \frac{LS\Omega}{E} \quad (4.5)$$

where $S = \pi \left(\frac{d}{2}\right)^2$ is the area of the entrance of the fibre, $\Omega = 2\pi(1 - \cos\theta)$ is solid angle and $\theta = \sin^{-1}(NA)$.

So in the case for the ALPS-II, the wavelength is at 1064nm and the optical fibre has a diameter of 8.1μm. By comparing the two methods, we could conclude whether our simulation is consistent or agree in the same scale and to get a better understanding of how many black photons might enter the fibre and disturb our signal outcome. The simulation was done by comparing the rate of black body photons with two methods within the temperature range from 15°C to 30°C.

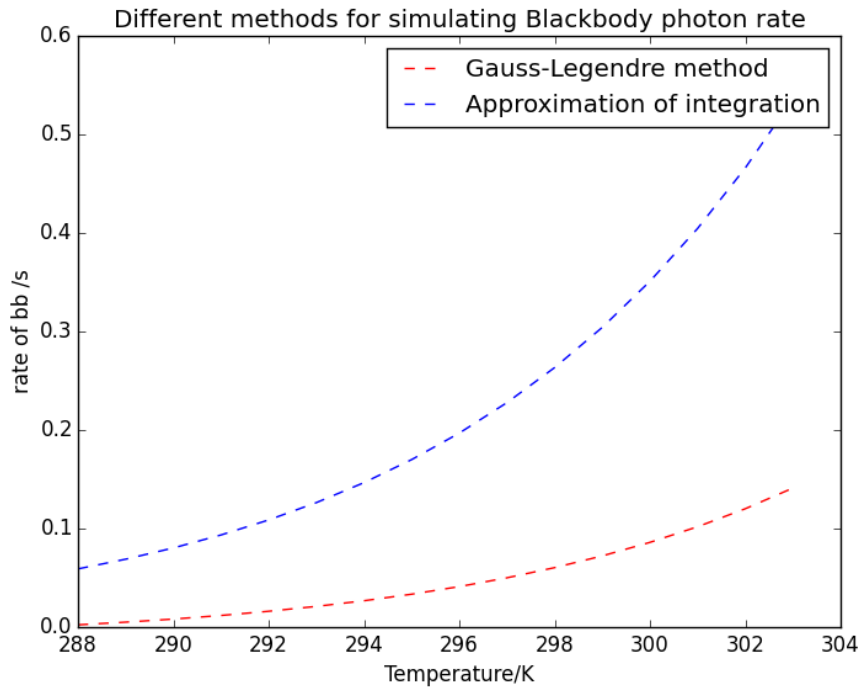


Figure 14: Simulation of black body photons entering the fibre with two methods.

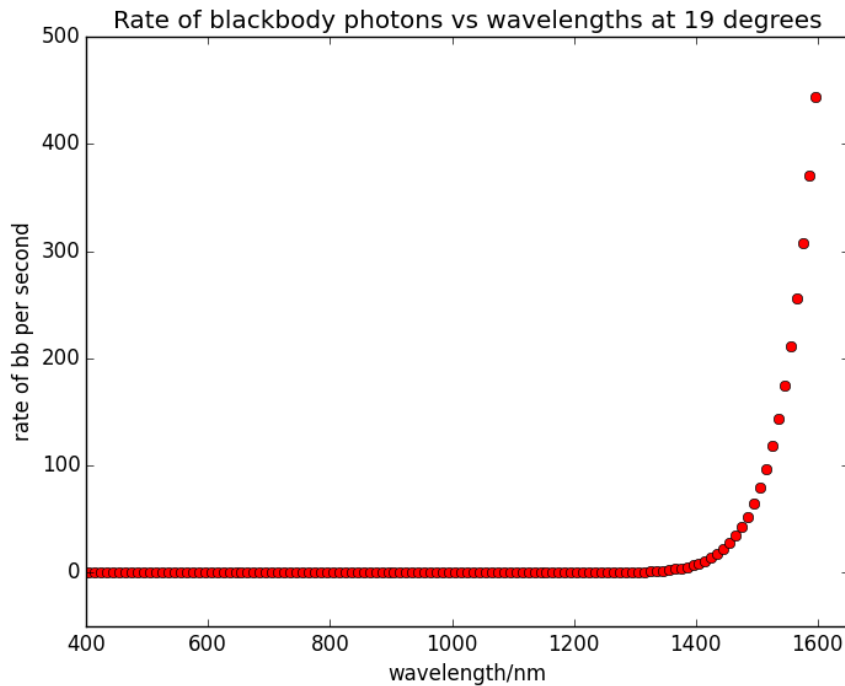


Figure 15: The rate of black body photons against wavelengths at lab temperature 19°C.

It was observed that the two methods were not consistent. The primary reason for this would be that the approximation and the assumption for the first method was not valid in this temperature range. In the following simulations, we will stick with the Gauss-Legendre method for evaluating the black body photons. Another observation from the simulation is that the rate of black body photons increases almost exponentially according to the wavelength. Thus, the photons with higher wavelength could be the dominating background.

4.3 Investigation of the black body photons sources

The investigation was performed by using an inferred camera to capture the heating sources around the detector. And the simulation using Gauss-Legendre method was used to evaluate the number of photons produced by these sources.

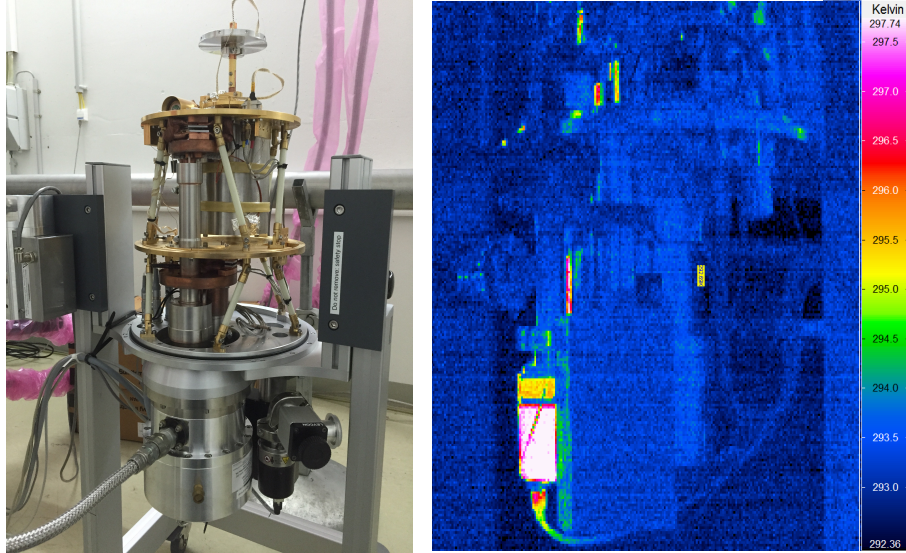


Figure 16: The picture of detector taken by IR camera with temperature scale.

For the components on the detector, the pressure sensor has a temperature of 297.74K and it is turned on all the times. More importantly, it is close to the black box where the fibres are connected into, and the inferred emitted by the pressure sensor might enter the fibre and produce the unexpected signal. Below is a summary of temperature readings for the surroundings of the detector and a simulation on the corresponding rate of black body photons.

	Environment	Pressure sensor	Computer Screen	Control system	Oscilloscope	Light
Temperature /K	293.0	297.7	301.8	303.7	306.6	311.2
L/E (W m ⁻² sr ⁻¹ J ⁻¹) for 1064nm	0.78×10 ⁶	1.59×10 ⁶	2.90×10 ⁶	3.81×10 ⁶	5.68×10 ⁶	10.79×10 ⁶
Rate of bbp (s ⁻¹)	1.57×10 ⁻³	3.21×10 ⁻³	5.85×10 ⁻³	7.69×10 ⁻³	11.50×10 ⁻³	21.80×10 ⁻³
L/E (W m ⁻² sr ⁻¹ J ⁻¹) for 1550nm	0.35×10 ¹²	0.58×10 ¹²	0.88×10 ¹²	1.06×10 ¹²	1.40×10 ¹²	2.18×10 ¹²
Rate of bbp (s ⁻¹)	712.9	1169.9	1771.6	2140.2	2821.3	4397.2

Figure 17: Table of the dominating heating bodies around the detector with simulation on the rate of black body photons produced by these objects.

The L/E is the spectral radiance per photon energy, it is irrespective to the shape of the heating body.

The rate of black body photons with wavelength of 1550nm is much larger than the the ones for 1064nm. It is very likely that the unexpected readings for 1550nm peak could come from these

heating bodies. Thus, in order to protect the fibre from other sources of inferred photons with 1550nm, a light-tightness shielding was made and tested with the inferred camera. The conclusion with the test is that the shielding is good enough to protect the fibre from the other sources of inferred photons so that the contributions apart from the pressure sensor and the environment can be eliminated.

4.4 Temperature gradient of the optical fibre

In order to make an estimation of how far and how long would it take for the optical fibre to have the same temperature as the environment between the 70K and the 4K stages of the ADR, the fibre was placed between a hot body and a cold body to investigate the temperature gradient.

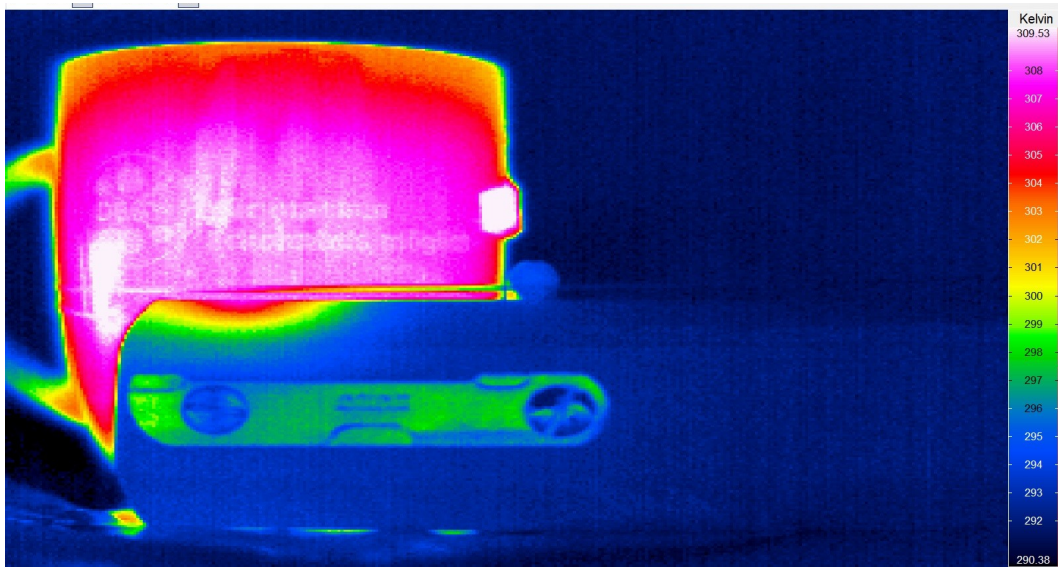


Figure 18: Temperature gradient of the fibre with a hot body and a cold body.

The length of which the fibre to be cooled to room temperature is 4.5 ± 0.2 cm and the time taken for this to happen was less than 1 second. However, one needs to take into account that the hot body also creates a temperature in the air as well. Therefore, we can conclude that in vacuum, it will take at most 4.5 cm for the fibre to decrease its temperature by 20K but the time taken for this to happen can be neglected.

4.5 Mechanical test for the protection of the optical fibre

Since the optical fibre is fed into the detector from outside, it is weak and dangerous without a protection. Therefore, a protection is demanded to protect the fibre while keeping its efficiency.

The mechanical test was performed by placing the fibre on the ground with a robust plastic tube for a week, with people stepping on it to imitate a more extreme scenario when placing outside the cryostat. Readings for the output from the optical fibre were measured before and after the mechanical test to see if there are any losses in efficiency. Each measurement was measured for 2 minutes.

The output power before the test was measured to be $811.0 \pm 0.3 \mu\text{m}$. The output power after the test was measured to be $808.3 \pm 0.3 \mu\text{m}$. Thus, the efficiency was dropped by approximately 0.3% which can be explained by the fluctuation from the laser and the set up.

Another advantage of using a robust protection is that it will protect the fibre from over-curving which will decrease the efficiency and people can clearly see the position of the fibre and would pay more attention when walking pass the detector. Since the plastic tube is not so heavy, it will protect the fibre without damaging it. However, one needs to be care of the ends of the protection where they connect with the parts of the fibre. These places will be the weakest parts of the protection. In conclusion, this type of protection is good enough to prevent the optical fibre from being damaged while maintaining the optical efficiency.

This experiment reminds me of another possibility that has not been though of. In the quantum efficiency tests, the fibre was directly connected to a laser source and sent photons to the TES. After a while the laser becomes warm, and this could explain the unexpected peak in 1550nm. Nevertheless, the TES is still under repair and a test could be done later on this to see if the intensity of the 1550nm peak has changed.

5 Conclusion

From the theory to detector, this summer internship has offered me a great experience in all the aspects of ALPS-II. It helps me to get an overview of the whole project and has significantly improved my research ability. Through the theory calculations, I could finally apply my knowledge from the text book to a more advanced topic, in this case, using Lagrangian and Feynman diagram to calculate the wavefunction of the probability for a pseudoparticle. From optics, I gained more experience in aligning optical components and a deeper understanding of the Gaussian beam and cavity. In the detector studies, I have developed my skills in simulating physics phenomena and also in problem solving. I become more familiar with hardware especially in building electronics.

Acknowledgement

Firstly, thank to the DESY summer program for offering such a good research experience for us and had a chance to meet lots of young scientists coming from all over the world. Not only the work here is nice, but also the people here are friendly and helpful.

Secondly, huge thanks to all the people from ALPS group. I really felt welcome and enjoyed working with you. As I am the only summer student in ALPS, I had a chance to touch all the fields inside the group. This broadened my knowledge and skills, and had a taste of what other research are like besides detectors. Thanks to Axel Lindner, the spokesperson of ALPS, for caring both my life and academic work at DESY. For the theory studies, many thanks to Andreas Ringwald for teaching me the idea behind the project and also the calculations for axion particle. For the optics, thanks to Aaron Spector, Jan Hendrik Pold, Christoph Weinsheimer and Natali Kuzkova. For detector studies, a huge thanks to Noemie Bastidon for all the efforts. Also thanks to other people who gave me support during my stay at DESY. This is the best research experience I had.

Reference

- [1] E. Masso and J. Redondo, Phys. Rev. Lett. 97(2006) 151802 [arXiv:hep-ph/0606163].
- [2] Robin Bahre, Babette Dobrich etc., *Any Light Particle Search II Technical Design Report*, arXiv:1302.5647v2 [physics.ins-det] 2 Aug 2013.
- [3] P. A. R. Ade, N. Aghanim, C. Caplan,(Planck Collaboration) et al. *Planck 2013 results. I. Overview of products and scientific results – Table 9*, Astronomy and Astrophysics 1303:5062, arXiv:1303.5062.
- [4] D. Clowe et al., *A Direct empirical proof of the existence of dark matter*, Astrophys.J. 648(2006) L109-L113, arXiv:astro-ph/0608407 [astro-ph].
- [5] H. Goldberg, *Constraint on the photino mass from cosmology*, Phys. Rev. Lett. 50 (1983) 1419.
- [6] J. Ellis et al., *Supersymmetric relics from the big bang*, Nucl. Phys. B238 (1984) 453-476.
- [7] J.D. Vergados et al., *Theoretical direct WIMP detection rates for transitions to nuclear excited states*, Phys. Rev. D 92, 015015 (2015), arXiv:1504.02803 [hep-ph].
- [8] E. Witten, Phys. Lett. B 149, 351 (1984).
- [9] J. P. Conlon, JHEP 0605, 078 (2006).
- [10] P. Svrcek and E. Witten, JHEP 0606, 051 (2006).
- [11] A. Arvanitaki, S. Dimopoulos, S. Dubovsky, N. Kaloper and J. March-Russell, Phys. Rev. D 81, 123530 (2010) [arXiv:0905.4720 [hep-th]].
- [12] G. Raffelt and L. Stodolsky, *Mixing of the photon with low-mass particles*, Phys. Rev. D 37 (1988) 1237.
- [13] M. Ahlers, H. Gies, J. Jaeckel, and A. Ringwald, *Light from the Hidden Sector*, Phys. Rev. D75, 035011 (2007), hep-ph/0612098.
- [14] P. Sikivie, Phys. Rev. Lett. 51 (1983) 1415 [Erratum-ibid. 52 (1984) 695].
- [15] A. A. Anselm, Yad. Fiz. 42 (1985) 1480.
- [16] M. Gasperini, Phys. Rev. Lett. 59 (1987) 396.
- [17] K. Van Bibber, N. R. Dagdeviren, S. E. Koonin, A. Kerman, and H. N. Nelson, Phys. Rev. Lett. 59, 759 (1987).30
- [18] A. Dupays, C. Rizzo, M. Roncadelli and G. F. Bignami, Phys. Rev. Lett. 95, 211302 (2005) [arXiv:astro-ph/0510324].
- [19] L. B. Okun, Sov. Phys. JETP56, 502 (1982).
- [20] B. Holdom, Phys. Lett. B166(1986) 196.
- [21] K. Ehret et al.[ALPS collaboration], Nucl. Instrum. Meth. A612, 83 (2009)[arXiv:0905.4159 [physics.ins-det]].
- [22] K. Ehret et al., Phys. Lett. B689(2010) 149 [arXiv:1004.1313 [Unknown]].
- [23] T.Erber [Nature(London) 190, 25 (1961)]
- [24] W. -Y. Tsai and T. Erber, Phys. Rev. D 12, 1132 (1975); R. Novick, M. C. Weisskopf, J. R. P. Angel, and P. G. Sutherland, Astrophys. J. 215, L117 (1977)
- [25] S. L. Adler, Ann. Phys. (N. Y.) 67, 599 (1971).
- [26] W. Heisenberg and H. Euler, Z. Phys. 98, 714 (1936)
- [27] K. R. Dienes, C. F. Kolda and J. March-Russell, Nucl. Phys. B 492 (1997) 104 [arXiv:hep-ph/9610479].
- [28] Paola Arias and Andreas Ringwald, *Illuminating WISPs with photons*, DESY 11-170, 11 Oct 2011, arXiv:1110.2126[hep-ph]

- [29] H. Kogelnik and T. Li, *Laser beams and resonators*, Appl. Opt. 5 (10), 1550 (1966)
- [30] P. A. Bélanger, *Beam propagation and the ABCD ray matrices*, Opt. Lett. 16 (4), 196 (1991)
- [31] Pampaloni, F. and Enderlein, J. (2004). *Gaussian, Hermite-Gaussian, and Laguerre-Gaussian beams: A primer*. arXiv:physics/0410021 [physics.optics].
- [32] K. D. Irwin and G. C. Hilton, *Transition-edge sensors, Cryogenic Particle Detection*, ed. C. Enss, Springer-Verlag (2005)
- [33] A. Lita *et al.*, *Counting near-infrared single-photons with 95% efficiency*, Optics Express 16, 3032 (2008)
- [34] A. Miller, S. Nam, J. Martinis, and A. Sergienko, *Demonstration of a low-noise near-infrared photon counter with multiphoton discrimination*, App. Phys. Lett. 83 (JUL 28, 2003) 791–793.
- [35] J. Clarke and A. I. Braginski (Eds.) (2004). *The SQUID handbook 1*. Wiley-Vch.
- [36] P. Sikivie, D. Tanner, and K. van Bibber, *Resonantly enhanced axion-photon regeneration*, Phys.Rev.Lett. 98 (2007) 172002, [hep-ph/0701198]
- [37] A. J. Miller, A. E. Lita, B. Calkins, I. Vayshenker, S. M. Gruber, and S. W. Nam, *Compact cryogenic self-aligning fiber-to-detector coupling with losses below one percent*, Opt. Express 19 (May, 2011) 9102–9110
- [38] Adkins, C. J. (1983). *Equilibrium Thermodynamics* (3rd ed.). Cambridge University Press. ISBN 0-521-25445-0.
- [39] Golub, Gene H.; Welsch, John H. (1969), *Calculation of Gauss Quadrature Rules*, Mathematics of Computation 23 (106): 221–230,